A.A. Bogdanov V.K. Chernyatin
R. Chrien I.V. Glavanakov
V.A. Grigoriev W. Gurin
G.N. Dudkin V.M. Emelyanov
V.A. Kaplin A.I. Karakash
Yu.F. Krechetov G.A. Naumenko
S.B. Nurushev A.P. Potylitsin
V.N. Padalko M.F. Runtzo
A. Russek M.N. Strikhanov

008-2000

THE INELASTIC SCATTERING DETECTOR OF PP2PP EXPERIMENT AT RHIC

Moscow 2000

MINISTERY OF EDUCATION OF RUSSIAN FEDERATION
MOSCOW STATE PHYSICAL ENGINEERING INSTITUTE
(Technical University)

A.A. Bogdanov V.K. Chernyatin R. Chrien I.V. Glavanakov
V.A. Grigoriev W. Guryn G.N. Dudkin V.M. Emelyanov
V.A. Kaplin A.I. Karakash Yu.F. Krechetov G.A. Naumenko
S.B. Nurushev A.P. Potylitsin V.N. Padalko M.F. Runtzo
A. Russek M.N. Strikhanov

The Inelastic Scattering Detector of pp2pp Experiment at RHIC

Preprint 008-2000

Approved by editorial board of the Institute

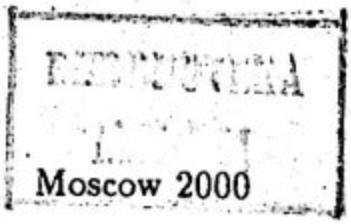

Moscow 2000

UDC 539.1.074
BBC 22.38
I59

Bogdanov A.A.[1], Chernyatin V.K.[2], Chrien R.[2], Glavanakov I.V.[3], Grigoriev V.A.[1], Guryn W.[2], Dudkin G.N.[3], Emelyanov V.M.[1], Kaplin V.A.[1], Karakash A.I.[1], Krechetov Yu.F.[3], Naumenko G.A.[3], Nurushev S.B.[1,4], Potylitsin A.P.[3], Padalko V.N.[3], Runtzo M.F.[1], Russek A.[2], Strikhanov M.N.[1]

[1] *Moscow Engineering Physics Institute, Russia.*
[2] *Brookhaven National Lab., Upton, NY, USA.*
[3] *Tomsk Institute of Nuclear Physics, Russia.*
[4] *Institute for High Energy Physics, Protvino, Russia.*

The Inelastic Scattering Detector of pp2pp Experiment at RHIC.

Moscow: preprint / MEPhI, 008-2000, - 36 p.

Abstract

Experiment pp2pp at RHIC aims to measure the total cross section and elastic pp-scattering (polarized and unpolarized) in the energy range $50 \leq \sqrt{s}\ (GeV) \leq 500$. The Inelastic Scattering Detector (ISD) is foreseen for counting events in the whole solid angle of the inelastic cross section σ^{in}. It will be also used for measurements of charged particle multiplicity and for vertex reconstruction of events. Some parts of the ISD will also monitor collider luminosity. One of the major goals of the ISD is to veto the elastic trigger accompanied by the background particles. Separately the Elastic Scattering Detector (ESD) installed in the Roman Pots (RP) will count the elastic scattering rate. By combination of data from ESD and ISD one can extract the total and differential cross sections. In this paper we present a detailed description of the ISD.

Introduction

The pp2pp Experiment at RHIC [1] plans to measure the pp - total and elastic scattering cross sections, including the determination of slope parameter b and the ratio of real to imaginary part of spin nonflip amplitude ρ at forward direction. With the advent of polarized proton beams all these measurements will be extended in order to include the spin physics study in the region of RHIC energy ($50 \leq \sqrt{s}\,(GeV) \leq 500$). To reach such a goal the pp2pp collaboration is building two types of detectors: the main detector, Elastic Scattering Detector, with high space resolution for measurement of pp - elastic cross section in the wide interval of invariant momentum transfer $-t$ ($10^{-3} \leq -t\,((GeV/c)^2) \leq 1.2$) and the Inelastic Scattering Detector. The latter will be used for independent measurement of inelastic cross section. Another function of ISD will be to veto the trigger for ESD in the case of inelastic scattering background. A third function of ISD will be to serve as a relative luminosity monitor (LM). The ISD counters are useful also in the case of tuning colliding proton beams in the Interaction Point (IP), for example, for measurement the charged particle multiplicity, for reconstruction of the event vertex, in the process of luminosity measurement by van der Meer (VDM) technique [2] or by fast wire scanning method [3], [4], in passing from the RHIC normal operation mode to the Terwilliger mode [5]. This paper is devoted to the detailed description of ISD for pp2pp experiment at RHIC. The first section briefly reviews the known schemes of σ_T measurement, the second one describes the running conditions and the third section is devoted to the ISD realization scheme. The radiation level estimates are presented in Section 4. The fifth one presents the Cathode Strip Chambers serving for the vertex reconstruction, the multiplicity measurement and the precise estimation of the inelastic scattering cross section. Section 6 features the data acquisition, electronics and triggers and section 7 underlines the experimental procedure and scheme of data analysis. The possible corrections to the observed total cross section σ_{obs} are discussed in section 8. The concluding paragraph summarizes the main results of this study.

1 The Survey of Schemes of Total Cross Section Measurements

The total cross section measurements at colliders (ISR, $Sp\bar{p}S$ and Tevatron) have been made by four methods. They are the followings:

1.1. The direct method. This means the measurement of the total interaction rate

$$N_T = N^{el} + N^{inel}, \tag{1}$$

where N^{el} and N^{inel} are the total elastic and inelastic rates respectively. The apparatus must cover 4π solid angle. In reality the vacuum pipe in colliders puts a limit on the minimum acceptable angle θ_{min}. Therefore, the measurements are done up to this angle and then one makes an extrapolation to correct the σ_{obs} for undetected events. Sometimes to improve the precision of measurements one uses an extension of ISD using Roman Pots (RP) and thus allowing to reach the smallest angles. Assuming that the machine luminosity L is known from an independent measurement, the total cross section can be determined through the relation

$$\sigma_T = N_T/L. \tag{2}$$

The examples of such a direct measurement of σ_T are presented in Table 1, column I, taken from experiments [6], [7]. It is evident, that the precision in σ_T of order 0.5 - 1 % can be reached only by special techniques, like using the Terwilliger scheme (to diminish a beam size), beam scrapers (to decrease the beam emittance), the precise measurement of beam luminosity L by the van der Meer method and the sophisticated apparatus (> 400 channels of scintillation counters). Moreover the elastic events were measured by a separate apparatus installed at small angles.

1.2. The indirect method. This is based on the optical theorem relating the differential cross section of pp nuclear elastic scattering in forward direction $\left(\frac{d\sigma^{el}}{dt}\right)_{t=0}$ and the total cross section σ_T (see Fig. 1):

$$\left(\frac{d\sigma^{el}}{dt}\right)_{t=0} = \frac{\sigma_T^2(1+\rho^2)}{16\pi(\hbar c)^2}. \tag{3}$$

Usually the differential cross section $\frac{d\sigma^{el}}{dt}$ is parameterised in the region of nuclear scattering (see region III in Fig. 1) as

$$\frac{d\sigma^{el}}{dt} = \left(\frac{d\sigma^{el}}{dt}\right)_{t=0} e^{-bt}, \tag{4}$$

were b is a slope parameter. Therefore, $\left(\frac{d\sigma^{el}}{dt}\right)_{t=0}$ should be defined by extrapolation of elastic events (measured) $\frac{dN^{el}(t)}{dt}$ to the $t = 0$ point:

$$\frac{dN^{el}(t)}{dt} = L \cdot \frac{d\sigma^{el}}{dt} = L\left(\frac{d\sigma^{el}}{dt}\right)_{t=0} \cdot e^{-bt} = \frac{dN^{el}(0)}{dt} \cdot e^{-bt}, \tag{5}$$

where

$$\frac{dN^{el}(0)}{dt} = L \cdot \left(\frac{d\sigma^{el}}{dt}\right)_{t=0}. \tag{6}$$

From relations (3) and (6) one can extract

$$\sigma_T = \frac{1}{\sqrt{L}}\left[\frac{16\pi(\hbar c)^2}{(1+\rho^2)} \cdot \left(\frac{dN^{el}}{dt}\right)_{t=0}\right]^{1/2}. \tag{7}$$

So taking L, luminosity, and ρ values from independent measurements, one can determine σ_T. The fractional error in σ_T due to the uncertainty in the luminosity is half of that in the first method. This is the simplest way to determine σ_T. The examples are presented in Table 1, column II [8], [9], [10]. Comparing with the previous example one can see that the precision of σ_T is not so good in this case as it was in the direct method. The most limiting contribution comes from uncertainty in the luminosity L measurements.

1.3. The Combined Method. In order to avoid the luminosity measurement, the following technique was invented ([11], [12]). From (2) and (7) one gets an expression without luminosity

$$\sigma_T = \frac{16\pi(\hbar c)^2}{(1+\rho^2)N_T}\left(\frac{dN^{el}}{dt}\right)_{t=0}. \tag{8}$$

Two types of detectors, ESD and ISD, must be used in this case. Additionally it is assumed that ρ is known. The results of using such method are given in column III. It is seen that the precision of σ_T measurement is better than in the column II.

1.4. The Coulomb Scattering. This method is based on the theoretically very reliable differential cross-section (see Fig. 1, region I)

$$\frac{d\sigma_c(t)}{dt} = \frac{4\pi\alpha^2(\hbar c)^2}{t^2}F^4(t), \tag{9}$$

where α is fine structure constant and $F(t)$ is the proton electromagnetic form factor. Its application requires access to the Coulomb scattering region,

which sits at $|t| < |t_0|$, where $|t_0| = 1.6 \cdot 10^{-3}\ (GeV/c)^2$ (for $\sigma_T = 40\ mb$), a point where the Coulomb cross section is equal to the nuclear one. Since $|t_0|$ is practically constant at a varying initial momentum p_{in} the Coulomb scattering angle must be smaller than

$$\theta_0\ (mrad) = \frac{\sqrt{|t_0|}}{p_{in}} \approx \frac{42}{p_{in}}. \qquad (10)$$

For ISR momentum $p_{in} = 15\ GeV$ we can find the value $\theta_0 \leq \frac{42 \cdot 10^{-3}}{15} \approx 3\ mrad$. This corresponds to the displacement of the scattered proton from the beam axis of about 3 cm at the end of the ISR 10 m long straight section. The experiment [13] was able to use this technique at two energies $\sqrt{s} = 23\ GeV$ and $\sqrt{s} = 31\ GeV$ at the base of the 10 m space. Reference [13] states "As it was impossible to operate at angle smaller than 2 mrad, the Coulomb measurements could not be performed for beam momenta above 15.4 GeV/c". The results of this experiment are presented in Table 1 (column IV); 2 % precision in σ_T measurement is a good achievement. But according to the relation (10) this method can not be directly used at higher energies. The modification of this technique using the accelerator lattice structure and a high β^* insertion was successfully applied at the $Sp\bar{p}S$ [10] and the Tevatron [14] for measuring the ρ-parameter. But in these experiments the absolute normalization comes from direct luminosity measurements, not from the Coulomb cross section. No publication using this method for σ_T measurement at $Sp\bar{p}S$ and Tevatron exists. Presumably, it is a difficult technique for application.

The simplest and reliable method is a direct measurement of σ_T; we must use both types of detectors: ESD and ISD and make a precise measurement of luminosity.

Table 1: Summary of experimental data on σ_T measurements

Facility, reaction, experiment.	$\sqrt{s}$ GeV	σ_T, mb I Dir. Meth.	II Indir Meth.	III Comb. Meth.	IV Coul. Scat.	Ref.
Tevatron, $p\bar{p}$ E710	1800			72.1 ±3.3		[11]
	1800	78.3 ± 5.9				[7]
CDF	546			61.26 ±0.93		[12]
	1800			80.03 ±2.24		[12]
	1800		72.0 ±3.6			[8]
SpS UA1	540		67.9 ±5.9			[9]
UA4	541		63.0 ±1.5			[10]
ISR (R210)						
pp	30.6	40.22 ± 0.21				[6]
pp	52.6	43.01 ± 0.27				
pp	62.7	43.82 ± 0.30				
$p\bar{p}$	30.6	42.8 ± 0.35				
$p\bar{p}$	52.8	44.71 ± 0.46				
$p\bar{p}$	62.7	45.14 ± 0.38				
pp	23.0				38.9 ±0.7	[13]
pp	31.0				40.2 ±0.8	

2 The Running Conditions

Three different running conditions are foreseen for the pp2pp experiment. They are as follows.

1. Total cross-section measurements in the energy interval $50 \leq \sqrt{s}$ $(GeV) \leq 500$. Such measurements can be done at the first stage of operation of RHIC since one can use low intensity beams, $L \approx 10^{31}\ cm^{-2}s^{-1}$. The accelerator tune at the crossing point may be a standard one with $\beta^* = 10\ m$. The elastic scattering up to $|t| \approx 0.15\ (GeV)^2$ has to be measured simultaneously as it was discussed in the previous section. This is necessary in order to extract the total cross section from raw counting rates. The normalized emittance is expected to be of order $\varepsilon_N = 20\ \pi\ (mm \cdot mrad)$.

2. Elastic differential cross section measurements in the Coulomb-nuc lear interference (CNI) region. A special tune of RHIC must be achieved to get the transverse betatron function $\beta^* = 195\ m$. In this case the luminosity is supposed to be of order $L = 10^{29}\ cm^{-2} \cdot s^{-1}$ and $\varepsilon_N = 5\pi\ (mm \cdot mrad)$.

3. High luminosity polarized beams. The elastic scattering and polarization measurement will be done at luminosity $L = 2 \cdot 10^{32}\ cm^{-2} \cdot s^{-1}$ with the goal of reaching the highest p_T region. The normalized emittance is supposed to be kept on the level of $20\pi\ (mm \cdot mrad)$. The special tool - polarimeter will be used for quantitative measurements of both beam polarizations which are expected to be of order 70 - 80 %.

The above information allows us to calculate the beam parameters which are presented in the following Table 2 for the 3 listed above running conditions. In this table σ_z means a "diamond" size in z (beam) direction, $\Delta p/p$ - beam momentum spread, P_B - beam polarization.

Table 2 shows the main beam parameters which are essential for proper detector design. For example, in the energy range of RHIC $50 \leq \sqrt{s}\ (GeV)$ ≤ 500 the yields of charged particles and their mean multiplicity are noticeably changing (Fig. 2, data are taken from Fig. 36.9 in [15], p. 186, the open circles for $\sqrt{s} = 200\ GeV$ and black circles for $\sqrt{s} = 546\ GeV$). The scenario 2 (column 3) shows that the small normalized emittance ε_N and the large beta function β^* are strong prerequisite in order to get a parallel beam for CNI measurement, though losing in luminosity.

Since our goal is to cover by Inelastic Scattering Detector a whole solid angle around the Interaction Region (IR) one needs move the detector closer to the maximum rapidity region which is

$$y_{max} \simeq \eta_{max} \simeq -ln\frac{\sqrt{s}}{mc^2}. \qquad (11)$$

Table 2: Beam parameters.

Scenario #	1	2	3
$\sqrt{s}, GeV$	200	500	500
$\beta_x^* = \beta_y^*,\ m$	10	195	10
$\varepsilon_N,\ mm \cdot mrad$	20π	5π	20π
$\sigma_x = \sigma_y,\ mm$	0.55	0.78	0.36
$\sigma_x' = \sigma_y',\ \mu rad$	55	4	35.4
$L,\ cm^{-2}s^{-1}$	10^{31}	$2 \cdot 10^{29}$	$2 \cdot 10^{32}$
$\sigma_z,\ cm$	10	15	10
$\Delta p/p$	10^{-3}	10^{-3}	10^{-3}
$P_B, \%$	70	70	70

For $\sqrt{s} = 200\ GeV$ and $546\ GeV$ they are $y_{max}\ (200) = 5.36$ and $y_{max}\ (546) = 6.28$. But the existing experimental data cover the region ≤ 4.8 (Fig. 2). In order to make an extrapolation closer to $y_{max}(\sqrt{s})$ we made fits to the experimental data at $\sqrt{s} = 200\ GeV$ and $\sqrt{s} = 546\ GeV$ by the Gaussian function,

$$\frac{1}{\sigma^{in}} \cdot \frac{d\sigma^{in}}{d\eta} = a1 \cdot e^{-\frac{(\eta - a2)^2}{2(a3)^2}}. \qquad (12)$$

For the fit, only data at the falling edge were used. The parameters of the best fit are the following:

$$\begin{aligned}
&\underline{\sqrt{s} = 200\ GeV}: \\
&a1 = 2.76 \pm 0.07,\ a2 = 1.79 \pm 0.18,\ a3 = 1.83 \pm 0.13, \\
&\chi^2 = 1.03/d.o.f. \text{ for 12 points and} \\
&\underline{\sqrt{s} = 546\ GeV}: \\
&a1 = 2.97 \pm 0.12,\ a2 = 2.16 \pm 0.22,\ a3 = 1.87 \pm 0.15, \\
&\chi^2 = 0.77/d.o.f. \text{ for 11 points.} \qquad (13)
\end{aligned}$$

The fits are presented by solid lines in Fig. 2, while dotted lines are extrapolations by formulae (12) with parameters (13). The dot-dashed lines show

the linear extrapolations to η_{max}. The inelastic counting rate for each ISD counter can be estimated by the relation

$$\dot{n}_{in} = \frac{dN^{in}}{dt} = L \cdot \sigma^{in} \cdot \sum_{k=\eta_{min}}^{\eta_{max}} \left(\frac{1}{\sigma^{in}} \cdot \frac{d\sigma^{in}}{d\eta_k} \cdot \Delta\eta_k \right). \qquad (14)$$

Here $\sigma^{in} = \sigma_T - \sigma^{el}$ and summation must be done over the whole acceptance region of the detector (counter). The sum itself gives a mean charge multiplicity $\overline{n}$ in the accepted rapidity region. Later we shall use this relation.

Another important item is the relative contribution of inelastic and elastic cross-sections to total counting rate. As was discussed earlier one needs to measure both cross-sections and extrapolate them to the forward angle. We know how to do it: relation (14) furnishes a necessary tool for inelastic counting rate estimates. For elastic scattering we use the well known relation (4). In this approximation there is a relation between $\sigma^{el} = \int (d\sigma^{el}/dt)dt$, $(d\sigma^{el}/dt)_0$ and b:

$$\left(\frac{d\sigma^{el}}{dt} \right)_0 = \sigma^{el} \cdot b. \qquad (15)$$

The counting rate for elastic scattering can be presented in a way similar to (14)

$$\dot{n}_{el} = L \cdot \sigma^{el} \cdot \sum_{i=1}^{n} \left(\frac{1}{\sigma^{el}} \cdot \frac{d\sigma^{el}}{dt_i} \cdot \Delta t_i \right), \qquad (16)$$

or through relations (4), (15) and (16) one can write

$$\dot{n}_{el} = L \cdot \sigma^{el} \cdot b \cdot \sum_{i=1}^{n} \left(e^{-bt_i} \cdot \Delta t_i \right). \qquad (17)$$

In practical case $\dot{n}_{in}$ and $\dot{n}_{el}$ are measured by different detectors, subtending different kinematical regions and having different geometrical acceptancies ε_g^i. Therefore, to make a total counting rate one needs to take into account those factors, including the efficiencies ε_i

$$\dot{n}_T = \dot{n}_{el}/(\varepsilon_{el} \cdot \varepsilon_g^{el}) + \dot{n}_{in}/(\varepsilon_{in} \cdot \varepsilon_g^{in}) = L \cdot \sigma_T. \qquad (18)$$

In order to compare the expected counting rates $\dot{n}_{el}$ and $\dot{n}_{in}$ Fig. 3 presents their θ (angle in lab. system) dependences. The inputs in calculations were: $p = 100\ GeV/c$ ($\sqrt{s} = 200\ GeV$), $L = 10^{31}\ cm^{-2} \cdot s^{-1}$, full

geometric acceptances and 100 % detector efficiencies. It is seen that at this energy, at angle $\theta = 4$ mrad, the counting rates become equal. This angle corresponds to $t = -0.16\ GeV^2$. Therefore the counting rate at $|t| \leq 0.16\ GeV^2$ is dominated by elastic scattering and at $|t| \geq 0.16\ GeV^2$ is dominated by inelastic scattering.

3 The Inelastic Scattering Detector (ISD)

This apparatus will detect the charged hadrons in a 4π solid angle and needed with the Elastic Scattering Detector (ESD) for the following goals:

- to measure the inelastic cross-section;
- to measure the total cross-sections;
- to trigger for the diffraction dissociation processes;
- to produce a fast signal for vetoing a trigger for ESD in the case when an "elastic scattering" is accompanied by associated inelastic charged particles.

The following requirements must be fulfilled by ISD:

- covers almost 4π solid angle and furnish a "full inclusive" trigger;
- has a good time resolution (better than 1 ns) in order to detect mostly beam - beam interactions;
- has a vertex reconstruction ability with a precision of order σ_z (in beam direction) $\approx 100\ mm$, and in transverse to beam directions $\sigma_{x,y} \approx 1\ mm$. This must furnish a good identification of beam-beam events agalnst background;
- furnishes a relative monitor for beam luminosity measurement.

The rapidity interval which should be covered by ISD can be determined from the experience of UA4. At $\sqrt{s} = 0.55\ TeV$ (which is close to our upper energy limit at RHIC) the UA4 rapidity coverage [17] is shown in the Table 3. We expect to achieve a similar coverage in our experiment. The last column indicates the portion of inelastically produced particles escaping the detectors.

Table 3: The rapidity coverage for a fully inclusive trigger.

Experiment	$\sqrt{s}$, GeV	y_{beam}	η_{min}	η_{max}	$\Delta\eta$	$y_{beam}-\eta_{max}$	ΔN_{inel}, %
UA4	546	6.4	2.5	5.6	3.1	0.8	1 ± 0.3
pp2pp	500	6.3	2.82	5.43	2.6	0.5	1.3

The possible scheme of installation of ISD at 2 o'clock IR of RHIC is shown in Fig. 4a. The ISD is composed of 3 parts: the Central Detectors (CD1 and CD2) surrounding the Interaction Point (IP), the Forward Detectors FD1-FD10 covering the large rapidity region, and the tracking detectors consisting of Cathode Strip Chambers, CSC11-CSC23. The following inputs have been taken into considerations:

- the experimental beam pipes (EBPs) have the complicated structure [18]. To maximize the transparency for the experiments, the 1.5 m central sections of the EBPs were made of berillium (Be). The outer diameter (OD) of Be sections is 7.6 cm and the nominal wall thickness is 1 mm. The Be section is extended by aluminium (Al) tube of 7.6 cm OD and 1 mm thick wall up to the distance 407 cm from the Interaction Point (IP). Then Al section gets a conical shape and expands to OD = 13 cm at 518 cm. At this OD the Al section continues up to the end of EBPs (861 cm from IP). The space for the IDS installation is limited around IP by a distance 700 mm, limited by the ion and titanium sublimitation pumps;

- the apparatus must have a cylindrical symmetry, that is, cover a whole azimuthal angle and should be placed at radius $R_{\min} \geq 40\ mm (l \leq 3.0\ m)$ and $R_{\min} \geq 60\ mm (l > 3.0\ mm)$;

- the forward detectors must fit to the existing free space (≤ 8 m from IP).

In order to suppress the accidental counting rates it was decided to put any counter in coincidence with neighbour counters. It is also desirable to have a standard size for counters. Our approach is illustrated by Fig. 4b.

We fix the position of counter 9: $z(9) = 650\ cm$. The outer radius of any counter we also fix at $R3 = 8\ cm (l \leq 3.0\ m)$ or at $R3 = 10\ cm (l > 3.0\ m)$. The inner radius $R2$ depends on the beam pipe. $R2 = 4\ cm (l \leq 3.0\ m)$ or $R2 = 6\ cm (l > 3.0\ m$, detectors FD7 - FD10) (see comments above). The beam diamond size is taken as $= 3 \cdot \sigma_{beam} = \pm 30\ cm$. We require that the bottom side of counter 7 sits on line presenting an extreme upper angle determined by counter 9. Then position $z(7)$ of counter 7 is defined through relation (in cm)

$$z(n-2) = [z(n) - 30] \cdot R(n-2)_{\min} / R(n)_{\max} + 30, \qquad (19)$$

where $n = 9$. Positions of all odd numbered counters were determined through this relation and they are presented in Table 4. The position of counter FD8 is defined by requirement that it is to be placed just in the middle of counters FD7 and FD9. Then the position of even numbered counters are defined by similar relation (19). Counters FD10 were however placed at a fixed position since there was little freedom. In Table 4 are shown also the minimum and maximum angles and rapidities subtended by each counter assuming a pointlike IR (Interaction Region). The expected counting rates calculated according to relation (14) are also included in this table. The calculations were made for $\sqrt{s} = 500\ GeV$ and luminosity $L = 2 \cdot 10^{32}\ cm^{-2} \cdot s^{-1}$ (Version 3 of Table 2). Since $\sigma^{in} = 50\ mb$, it follows that $L \cdot \sigma_T = 10^7\ s^{-1}$.

FDs should fulfill several additional functions in the case of the unpolarized beam collision. First, they monitor beam luminosity. For that the FD9R (right) and FD9L (left) will produce a coinciding signals featuring the beam-beam collisions. At the first stage one makes an OR signal from each plane (FD8, FD9 and FD10) mixing with a good timing signals from 6 counters in each plane. So, we label them as S8, S9 and S10. In order to suppress noises we make coincidences $S8 \times S9$ and $S9 \times S10$ and then mix them. So we have a signal

$$T9 = S8 \times S9 + S9 \times S10. \qquad (20)$$

This presents a telescope. Similar signals will be shaped from other detectors. In order to avoid a firing from the background particles moving along the EBPs one plans to use a veto signal from T7 or T6:

$$V9 = T6 \times T7. \qquad (21)$$

So the right luminosity monitor will be arranged in the following way

$$M9R = T9R \times \overline{VR9}. \tag{22}$$

The coincidence of left and right telescopes will furnish a relative luminosity monitor

$$M9 = M9R \times M9L. \tag{23}$$

All above counting rates should be present in fast scalers. Situation becomes a little bit different in the case of collision of polarized proton beams. In this case we should keep in mind that the angular distributions of the secondary charged particles will in general follow the following azimuthal dependence

$$\begin{aligned} N(\Theta, E, \vec{P}_1, \vec{P}_2) = N_0(\Theta, E)[1 + P_1 A_{1N} \cos\varphi_1 + P_2 A_{2N} \cos\varphi_2 \\ + P_1 P_2 A_{1N} A_{2N} \cos\varphi_1 \cos\varphi_2]. \end{aligned} \tag{24}$$

Luminosity monitor shouldn't depend on the beam polarization. It means the monitoring counters must be placed at the position $\varphi_1, \varphi_2 = 90^o, 270^o$. That is, the luminosity monitor must be placed in the plane, which passes through a beam momentum and it's polarization vector. In the case of RHIC we expect to get polarization vector $\vec{P}_B$ either along $\vec{N}$ (normal to the horizontal plane) or $\vec{S}$ (in horizontal plane and it's directed perpendicular to the beam momentum $\vec{K}_e$). Therefore, for normally polarized beam $\vec{P}_N$ we should put monitor counters up and down in the vertical plane, while for the transversally polarized beam, $\vec{P}_S$, the monitor counters should be in the horizontal plane (left-right counters). If for some reason, the polarization stable direction is tilted from $\vec{N}$ and $\vec{S}$ direction the possible way revealing such effect is to install two additional counters at the azimuthal angles, let say, 45^o and 225^o. Such an approach leads us to the construction of FD6 counters, as shown in Fig. 5, and the counting rate is given for each counter.

Table 4 leads to the following conclusions:

- a very high counting rate is expected for each of 6 counters of cylindrical detector CD1 also the mean charged particle multiplicity is high;
- cylindrical detector CD2 has a lower rate due to fine segmentation;
- rates in other counters are tolerable.

Table 4: The detector positions l, rapidity η, and angular θ acceptances, the counting rates $\dot{n}$ and a mean charged particle multiplicity $\bar{n}$.

Detectors	l, cm	θ_{min},deg	θ_{max},deg	η_{min}	η_{max}	$\dot{n}$,MHz	$\bar{n}$
CD1	-	4.80	175.2	-3.18	3.18	33.6	3.36
CD2	-	4.80	175.2	-3.18	3.18	2.8	0.28
FD1	67.2	3.41	6.79	2.82	3.52	3.8	0.38
FD2	85.8	2.67	5.33	3.07	3.76	3.6	0.36
FD3	104.0	2.19	4.38	3.26	3.96	3.3	0.33
FD4	142.0	1.62	3.23	3.57	4.26	2.3	0.23
FD5	179.0	1.28	2.56	3.80	4.49	2.1	0.21
FD6	290.0	0.79	1.58	4.29	4.98	1.9	0.19
FD7	402.0	0.86	1.42	4.39	4.90	1.4	0.14
FD8	526.0	0.65	1.09	4.66	5.17	1.2	0.12
FD9	650.0	0.53	0.88	4.87	5.38	1.1	0.11
FD10	690.0	0.50	0.83	4.93	5.43	1.1	0.11
Comments: CD2 consists of 12x6=72 counters while C1 consists of only 6 counters.							

4 Radiation Level in ISD

According to reference [15], p. 152, "In a typical organic material, a relativistic charged particle flux of $3 \cdot 10^9\ cm^{-2}$ produces an ionizing radiation dose of $1Gy$" (where $1Gy = 1\ Joule \cdot kg^{-1}$). Therefore, in order to absorbe a dose of $1Gy$ assuming a homogeneous irradiation one must multiply the above number by the surface, S, of the counter of interest. For example, $S = 25.13\ cm^2$ for FD1. Then the flux $f = 3 \cdot 10^9 \cdot 25.13 = 0.81 \cdot 10^{11}$ must pass through FD1 for getting $1Gy$ absorbed dose. Since the counting rate expected is 3.9 MHz (see Table 4), then for a year's running the integrated dose will be $D = \frac{3.9 \cdot 10^6 \cdot 10^7}{0.81 \cdot 10^{11}} = 481\ Gy = 48.1\ krad$. Other counters will be irradiated at a lower dose level. Therefore, we do not expect any serious problem with irradiation of the ISD counters. In order to get some idea about the radiation level at RHIC in comparison with other colliders we borrowed the following Table 5 from [15] and expanded it by one column

designated RHIC. It is seen that the radiation condition is expected to be more severe than in TeVatron, but much better than in LHC.

Table 5: A rough comparison of beam-collision induced radiation at the different colliders.

Collider	RHIC	Tevatron	LHC	SSC	100TeV
$\sqrt{s}(TeV)$	0.5	1.8	15.4	40	100
$L_{nom} \cdot 10^{34}$ $(cm^{-2} \cdot s^{-1})$	0.02(a)	$2 \cdot 10^{-4}$	1.7(a)	0.1	1
$\sigma_{inel}(mb)$	50	56	84	100	134
H	3.0	3.9	6.2	7.5	10.6
$< p_\perp > (GeV/c)$	0.425	0.46	0.55	0.60	0.70
Relative dose (b)	$3.1 \cdot 10^{-2}$	$5 \cdot 10^{-4}$	11	1	20
Comments: a)High luminosity option. b) Proportional to $L_{nom} \cdot \sigma_{inel} \cdot H \cdot < p_\perp >^{0.7}$.					

5 The Cathode Strip Chambers (CSC)

There are several reasons for using the coordinate detectors in our case. They are followings:

- the event vertex reconstruction. This is important information for reducing the backgrounds originating out of the IR;
- the charged particle multiplicity measurements. This information is crucial in checking the dependence of inelastic cross section σ^{in} on the initial colliding energy which varies at RHIC from $\sqrt{s} = 50\ GeV$ up to $\sqrt{s} = 500\ GeV$. Assuming that $\sigma^{in}(pp)$ is equal to $\sigma^{in}(\overline{p}p)$ one can monitor also the measured inelastic cross sections by using the published data on $\sigma^{in}(\overline{p}p)$;
- the fine coordinate resolutions allow a check of the efficiency of scintillating counters of Forward Detectors and allow all necessary corrections during off-line analysis;

- the control of beam parameters. Due to the fine space and time resolutions and azimuthal symmetry, the coordinate detector allows control of such beam parameters as size, time and space stability. In the case of polarized proton beam they may check the transverse component of polarization by measuring the azimuthal distribution of charged particles, if the analyzing power differs from zero.

As the coordinate detectors we plan to use the Cathode Strip Chambers (CSC) developed for application at LHC [16]. Their attractive features are: high position resolution, good time resolution, and small dead time. An important advantage of the CSC technology is the flexibility in choosing the cathode pattern. This provides an opportunity to utilize the cylindrical symmetry relevant to pp2pp experiment. The sketch of one plane of CSC which can fit to our experimental environment is shown in Fig.6. The cathode strip is made as a ring accepting the fixed polar angle, while an anode wire is stretched in radial direction.

In such a way one takes into account the cylindrical symmetry of ISD. Since a pitch between anode wires varies from value S_{min} at radius R_{min} to S_{max} at radius of R_{max} (see Fig.6) it is necessary to vary also a gap H between anode and cathode planes. This must be done in order to keep a constant gain of signal. The gap between anode and cathode planes must respect the following relation

$$H = \frac{x \cdot H_{min}}{\pi} \cdot (\pi - lnx), \tag{25}$$

where $x = R/R_{min}$ is a ratio of current radius R to R_{min}. This function is a complicated one in order to realize it in practice. In the first approximation one can use a linear function

$$H_1 = H_{min} + \frac{(H_{max} - H_{min}) \cdot (x-1)}{x_{max} - 1},$$

where H_{min} is a minimum gap at $R = R_{min}$ between anode and cathode planes, H_{max} is a maximum gap at $R = R_{max}$. Then taking into account expression for H_{max} (assuming $x = x_{max}$) from formula (25), H_1 can be written as

$$H_1 = \frac{x \cdot H_{min}}{\pi} \cdot (\pi - \frac{x_{max}}{x_{max} - 1} \cdot \frac{x-1}{x} \cdot lnx_{max}). \tag{26}$$

The difference between two functions H_1 and H can be presented as

$$\Delta H = \frac{x \cdot H_{min}}{\pi} \cdot \left(\frac{x_{max}}{x_{max}-1} \cdot \frac{x-1}{x} \cdot lnx_{max} - lnx\right). \qquad (27)$$

The position x^* where ΔH has a maximum can be found by taking a first derivative and putting it as equal to zero

$$x^* = \frac{1}{e} \cdot (x_{max})^{\frac{x_{max}}{x_{max}-1}}. \qquad (28)$$

Now the maximum deviation from linearity ΔH_{max} can be calculated inserting x^* into expression (27).

The following Table 6 presents the results of such calculations. It shows that a linear approximation can be used as a practical solution up to $x_{max} = 4$, where the gain variation along radius is less than 2. Special spacers will be used to keep an appropriate gap between anode and cathode planes. To cover a whole range of interest in pseudorapidity ($2.2 \leq \eta \leq 5.0$, $0.79 \leq \theta^o \leq 12.6$), it is planned to use two stations of CSC's. The first one will cover the angular interval $3.2 \leq \theta^o \leq 12.6$ (corresponding pseudorapidity range is $2.2 \leq \eta \leq 3.6$) and the second station will subtend the angular interval $0.79 \leq \theta^o \leq 3.2$ ($3.6 \leq \eta \leq 5.0$). Let us describe more details.

Table 6: Estimates of some CSC parameters for pp2pp experiment.

Parameters	Magnitudes						
x_{max}	2.0	2.5	3.0	3.5	4.0	4.5	5.0
S_{min}, mm	2.0	2.0	2.0	2.0	2.0	2.0	2.0
S_{max}, mm	4.0	5.0	6.0	7.0	8.0	9.0	10.0
$H_{min} = S_{min}$, mm	2.0	2.0	2.0	2.0	2.0	2.0	2.0
x^*	1.51	1.70	1.91	2.12	2.34	2.35	2.75
H_{max}, mm	3.1	3.54	3.90	4.21	4.47	4.69	4.88
ΔH_{max}, mm	0.06	0.11	0.17	0.24	0.31	0.39	0.47
G_{max}/G_{min}	1.18	1.32	1.48	-	1.83	-	2.19

Each station consists of three chambers. In the first station the chambers are installed at distances from IP of 1.985 m, 2.235 m and 2.485 m. Taking into the account angular interval for the first station one can calculate for

the farthest chamber $R_{min} = 8\ cm$, $R_{max} = 45\ cm$ and $x = R_{max}/R_{min} = 5.625$.

If the second station chambers have the same sizes they should be installed at distances from the IP 3.675 m, 4.675 m and 5.675 m. In this case extrapolation accuracy into the IP region will be the same for both stations.

Assuming $S_{min} = 2\ mm$ (see Table 6) one can estimate a number of anode wires in each plane:

$$n_{aw} = \frac{2\pi R_{min}}{S_{min}} = 352. \qquad (29)$$

Assuming $\sqrt{s} = 200\ GeV$ one can estimate from ref. [18] the charged particle density per angle: 20 charged part./rad. for $0 \leq \theta^o \leq 5.7$. Each hit occupies 5 strips or 2.5 cm or 0.012 rad. Therefore occupancy is $20 \cdot 0.0125 = 0.25$. In this case 25% particles will hit into the cell occupied by another particle and therefore will be lost. This is not acceptable and therefore each strip should be divided to make it smaller. For instance if strips are divided by four sectors an occupancy reduces to 0.06. Additionally one gets rough information on an azimuthal angle too.

The number of electronic channels n_e can be estimated the following way: if $R_{max} - R_{min} = 33.5\ cm$, and the pitch = 0.5 cm, we have 4 sectors in the azimuthal angle, therefore $n_e = (33.5/0.5) \cdot 4 = 268$ for each chamber. For 6 chambers $N_e = 6 \cdot n_e = 1608$. Since the chambers must be symmetrically placed around the IP one must double this number, that is, the total electronic channel number will be 3216.

The precision at IP transverse to the beam plane, is expected to be 0.1 mm (detector resolution) $\cdot$ (1.75/0.25) $\cong$ 0.7 mm.

The vertex reconstruction precision along the beam axis depends on track inclination. In the worst case, at $\theta = 0.79^o$, the accuracy in the z direction, $dz = 50\ mm$; at $\theta = 12.5^o$ $dz = 3.2\ mm$. This precision is good enough to reject interactions out of the "diamond region" ($\pm 30\ cm$). An average multiplicity of charged particles in the solid angle subtended by CSC's is $\bar{n}_{ch} = 12$ at $\sqrt{s} = 500\ GeV$ and $\bar{n}_{ch} = 5$ at $\sqrt{s} = 50\ GeV$ (in one hemisphere). Therefore vertex reconstruction for real events should be much better than for a single track.

The simultaneous use of the FD's and CSC's allows efficiency measurements of both detectors using the alternative triggers from those detectors. In addition more detailed azimuthal charged particle distributions can be extracted.

Table 7: The Cathode Strip Chamber (CSC) parameters.

CSC	Distance from IP,m	Dimensions, mm		Angular interval,deg	η interval
		R_{min}	R_{max}		
CSC11	1.985	80	450	2.3 - 13.0	2.2 - 3.9
CSC12	2.235	80	450	2.1 - 11.5	2.3 - 4.0
CSC13	2.485	80	450	1.8 - 10.4	2.4 - 4.2
CSC21	3.675	80	450	1.25 - 7.0	2.8 - 4.5
CSC22	4.675	80	450	0.98 - 5.5	3.0 - 4.8
CSC23	5.675	80	450	0.81 - 4.5	3.2 - 5.0
Comment: The beam sizes were not taken into account.					

6 The Main Triggers, Electronics and Data Acquisition

We classify our detectors as a left or right arm depending on their positions relative to the interaction point. We take a clockwise rotating beam as a main reference axis and in this particular case, the downstream counters will be right and upstream ones left. Assuming that we get a synchronizing signal from accelerator the full inclusive (FI) trigger requires at least one track in any detector in one arm in coincidence with at least one track in any detector in the opposite arm

$$T^{FI} = (ARM)^{FI}_{L} * (ARM)^{FI}_{R}, \tag{30}$$

$$(ARM)^{FI}_{i} = (CD + FD1 + ... + FD10)_{i}, i = L, R. \tag{31}$$

PYTHIA v.5.7 and JETSET v.7.4 programs were used at $\sqrt{s} = 500\ GeV$ in order to estimate the geometrical efficiences (in %) of detectors to the charged particle events. For the positions of detectors fixed in Fig.4b (see Table 4) the efficiency for triggering by each counter is (in%): 83.8 (FD1), 85.2 (FD2), 81.7 (FD3), 78.7 (FD4), 76.7 (FD5), 73.1 (FD6), 70.2 (FD7), 65.1 (FD8), 60.3 (FD9), 60.7 (FD10). Total efficiency (any of 10 detectors will react) was 98.7%, therefore the geometrical inefficiency is 1.3% which is

shown in Table 3 too (it is consistent with UA4 data). If we require a coincidence of the left and right forward detectors according to the equation (30) then the estimated geometrical efficiencies are given in the Table 8.

Table 8: The geometrical efficiencies (in %) with triggering by left-right FDs on coincidences.

L/R	FD1	2	3	4	5	6	7	8	9	10
FD1	71	70	68	67	65	62	60	53	52	52
FD2	70	69	69	66	64	65	58	53	51	51
FD3	69	67	69	68	63	59	54	54	51	49
FD4	69	66	67	62	61	57	59	52	50	47
FD5	66	66	63	60	60	53	56	49	49	51
FD6	63	64	61	57	57	54	54	48	46	47
FD7	61	60	58	57	55	54	48	46	41	41
FD8	56	52	54	52	52	48	43	42	38	40
FD9	53	53	48	46	48	45	44	39	37	36
FD10	54	49	48	51	45	45	42	40	35	36

In each arm for suppression the accidental counting rates the signals from neighbour counters FDI (I=1,10) subtending the overlapping solid angles will be put in coincidence, and "or"-ed. In such a way the signals $(ARM)_L^{FI}$ and $(ARM)_R^{FI}$ will be formed. The timing of the main L*R coincidence (30) will be kept loose ($\Delta t = \pm 40\ ns$) to ensure collection of all good triggers and to admit some backgrounds for monitoring purposes. This trigger corresponds, by definition, to the observed cross section. The second main trigger will be arranged for elastic scattering events by coincidence of the left and corresponding right elastic counters. When a trigger occurs all relevant information will be transferred by CAMAC to the computer for subsequent analysis. This information will comprise: i) the hit pattern in all counters, ii) the arrival times of hodoscope signals with respect to the trigger, and iii) the live - time of the data acquisition prior to the trigger. The fast logic is inhibited during data acquisition. The electronics scheme is presented in Fig. 7. Each counter is furnished by discriminator and fanout, ADC and TDC electronics. Each signal is split in order to make: i) the coincidence with signal from a counter in the other plane, ii) the amplitude

analysis, and iii) the time-of-flight measurement.. The start time is given by a synchronizing signal and stop signal from each counter. A separate set of scalers will continuously count the rates of the main trigger, all detector coincidences, and various monitors. These scalers will be read and reset by the counters at fixed time intervals, typically every 0.1 seconds. The operating conditions of all counters, the electronics and the TOF and ADC logics will be controlled by the on-line data acquisition program and will be checked by means of special runs. During such run the data acquisition will be interrupted and fast flash-diodes attached to each counter will be pulsed. The triggering of these diodes will be computer controlled and they allow simulation of any event configuration. There are runs foreseen in which the main gate will be randomly triggered by a pulse generator in the same beam configurations as for data taking. Such special runs will allow measurements the random rates and the dead-time losses, both in the main trigger and in each of the hodoscope counter registers. The special accelerator regime will be used for study of running conditions in experiment, like the luminosity measurement, the estimates of single arm backgrounds, timing of counters etc.

7 The experimental procedure and analysis of data

The observed counting rates have to be corrected for backgrounds (including the accidental counting rates), and for missing events.

The backgrounds usually originate from single beam interaction with internal materials (vacuum pipe, a gas, any internal target, etc.), while the effects are due to the beam-beam interaction. The background will be studied in special runs with time of flight (TOF) method separating the beam-beam and the single beam events with a good time resolution (of order of several nanoseconds).

Pulses of all 6 counters in each plane are "or"-ed. Then the signals of two neighbouring planes are put in coincidence. These signals from adjacent planes are "or"-ed. So there are finally 5 output TOF signals.

Since we have 5 TOF outputs from each group of detectors (left or right) we can, in principle, compute 25 TOF's. The resolution of three classes of events beam-beam (BB), single beam 1 (SB1) and single beam 2 (SB2) in different TOF's is a function of the distances of both participating detectors from the crossing point.

The TOF spectrum of closest to IP detectors like FD1-FD3 (TOF pulse TR1 left minus TR1 right) must show the peaks from beam-beam (BB) and single -beams (SB1 and SB2) interactions. At the same time the time difference between TR5 (left) - TR5 (right) must show a clean BB signal, while SB1 and SB2 signals will be out of its range. For convenience, following [19], one transforms the TOF information into a set of dimensionless quantities

$$S_i^2 = \frac{(t_i - < t_i >)^2}{W_i^2}, \tag{32}$$

where $< t_i >$ and W_i are the centers and widths of the BB peaks in the i-th TOF and their values will be obtained in clean (BB) conditions. The widths are expected to be of order 2 - 6 ns depending on beam conditions and the position of detectors. The advantage of such a transformation lies in the simplicity with which any subset of the 25 TOF's could be summarized in a single number, or super - TOF (STOF) characteristic of the signature of the event:

$$S^2 = \sum_i^n S_i^2/n, \tag{33}$$

where the sum is performed over the n TOFs in subset. The STOF information will be classified according to the following Table 9.

Table 9: Classification of TOF information.

<table>
<tr><td colspan="2"></td><td colspan="6">Right</td></tr>
<tr><td colspan="2"></td><td>CD</td><td>TR1</td><td>TR2</td><td>TR3</td><td>TR4</td><td>TR5</td></tr>
<tr><td rowspan="6">Left</td><td>CD</td><td>S_d^2</td><td colspan="5">S_c^2</td></tr>
<tr><td>TR1</td><td rowspan="5">S_b^2</td><td colspan="4" rowspan="4">S_a^2</td><td rowspan="3"></td></tr>
<tr><td>TR2</td></tr>
<tr><td>TR3</td></tr>
<tr><td>TR4</td><td colspan="2" rowspan="2">S_m^2</td></tr>
<tr><td>TR5</td><td></td></tr>
</table>

The luminosity monitor will be derived from the S_m^2 STOF (see area in Table 9). S_m^2 will be defined for events in which at least one TOF will be

present within its domain regardless of the presence of TOFs outside it. In order to calibrate the luminosity monitor one uses the relation

$$R_M = \sigma_M \cdot L, \tag{34}$$

where R_M is the rate of the interactions that trigger the monitor and σ_M is the inclusive cross section for them. If the latter is known, the instantaneous luminosity can be derived directly from the monitor rate.

To calibrate a monitor the RHIC beams will be steered vertically (or horizontally) through each other, changing δ in small precise steps (0.5 or 1 mm) while recording $R_M(\delta)$. The calibration constant σ_M will be then found by evaluating the integral

$$\int R_M(\delta)d\delta = I_1 \cdot I_2 \cdot \sigma_M / K_{RHIC}: \tag{35}$$

Here I_1 and I_2 are the total currents of beams (they are measured to better than 0.1 %), K_{RHIC} is a constant parameter

$$K_{RHIC} = \frac{\beta e^2 c \cdot \sin(\frac{\alpha}{2})}{\sqrt{1-\beta^2 \cdot \sin^2(\frac{\alpha}{2})}} \cong \beta \cdot 0.2688 \cdot 10^{-29}(cm \cdot s \cdot A^2), \tag{36}$$

α is a crossing angle ($\alpha = 7mrad$ at RHIC), and βc is the velocity of colliding protons (in symmetrical beams). The signal R_M can be represented by a n-parameter function:

$$R_M(\delta) = \exp[a_1 - a_2(\delta - \delta_0)^2 + a_3(\delta - \delta_0)^3 + ... + a_{n-1}(\delta - \delta_0)^{n-1}]. \tag{37}$$

Parameters a_i, δ_0 will be extracted from a least-squares fit to the data. The function $R_M(\delta)$ will be then integrated numerically to get σ_M (see relation (35)).

The previous approach of using the van der Meer (VDM) method suffers from the following deficiency: the measured luminosity depends on the beam-beam crossing angle α (see formula (36)) through its inverse power. It means that VDM technique is not favorable for RHIC, since the ratio of the crossing angles is $\alpha(RHIC)/\alpha(ISR) = 1/28$.

Therefore one can think of a different approach to the luminosity measurement, as was done in paper [3]. Following approach [3] is justified by the relation for the instantaneous machine luminosity L_1 and other observables

$$L_1 = \sum\{(f \cdot N1_i \cdot N2_i)/[2 \cdot \pi \cdot (\sqrt{s1_i^2(x) + s2_i^2(x)} \cdot (\sqrt{s1_i^2(y) + s2_i^2(y)}]\}. \tag{38}$$

Here $N1_i$ and $N2_i$ mean the number of particles for each of colliding bunches and sum is taken over 57 RHIC bunches; $s1_i$ and $s2_i$ characterize widths of beam profiles for each beam; f is revolution frequency. The number of particles in each bunch will be measured by synchronous receivers placed at various positions around the collider. They should be absolutely calibrated with a precision better than 1 %, since they contribute directly to the total cross section precision. A precise measurement of the horizontal and vertical beam profiles and positions for each of 57 bunches (for both beams) will be done by a wire scan system placed at the crossing point [4]. Two data sets will be recorded for each bunch corresponding to two traversals in opposite directions of the wire through the beam. One expects to get a gaussian profile with a width (r.m.s.) of order 1 mm (see Table 2). Since the precision in the width measurement transforms directly to the accuracy in the total cross section measurement one must reach a beam width precision of order 1 %. This problem will be discussed in separate paper.

The analysis of STOF spectra showed [6] that almost all BB signals were contained in the region $S_a^2 < 2$ (A-region). A small fraction of the total amount of SB background was also found in that region. The part of the spectrum above $S_a^2 = 2$ (B-region) will be used to monitor the background R_B:

$$R_A(\delta) = R_M(\delta) + \beta R_B(\delta) = \sigma \cdot \Delta L + \beta R_B(\delta). \tag{39}$$

The coefficients σ and β will be obtained by a global fit of the R_A versus ΔL curve.

As one can see from last Table 9, the important triggers, TR4 and TR5, monitoring the beam luminosity, are built from pulses produced by the four last detectors FD7 $\div$ FD10 containing scintillating counters. The triggers S_b^2 and S_c^2 are sensitive to beam-beam and single beam interactions and they will be used for estimating of backgrounds.

The observed pp cross section will be measured as a part of the luminosity calibration; σ_{obs} will be obtained through the same procedure as that followed for σ_M, except that no cuts will be made on the STOF spectra to obtain the beam-beam rate; instead, the raw rate of the fully inclusive trigger (R_{inc}) will be used as

$$R_{inc}(\delta) = R_{obs}(\delta) + \beta R_B(\delta), \tag{40}$$

where the B region of the S_a^2 distribution is used to estimate the background R_B. S_a^2 presents all triggers in Table 9 (sometimes neglecting CD pulses).

Since one measures simultaneously the luminosity L, one can get

$$\sigma_{obs} = R_{obs}/L. \tag{41}$$

It may happen that for independent determination of constant β in (40) two measurements would be done: one with the beams fully overlapping and one with beams separated by 4 mm.

8 Background subtractions and corrections

After getting the σ_{obs} one must introduce several corrections and take into account the backgrounds. The major contributions are the following.

8.1 Background subtraction

The various TOFs will be treated in three different ways according to their features:

- there are TOFs free from single beam contamination (see Table 9, S_m^2). In this case the flat background will be subtracted from the beam-beam peaks by extrapolating the level observed away from the peaks. The events remaining inside some fiducial cuts after this subtraction will be accepted as good beam-beam events;

- there are TOFs showing single-beam peaks (see Table 9, S_b^2 and S_c^2). In this case the shape of the background peak will be measured in separate runs with only one beam circulating in RHIC. Later this shape will be added to a constant level with a free relative normalization, fitted to the TOF distribution in the region outside the beam-beam peak, and then subtracted from the spectrum;

- there is a background under beam-beam peak which can be subtracted by using TOFs including the CD-box. In such subtractions the average normalization factor found by the previous fits will be used.

8.2 Corrections

The main corrections to the observed cross section are expected to arise from two sources:

- the small-angle processes escaping the trigger due to the finite size of the vacuum pipe;

- the dead space between adjacent trigger counters.

1. The loss of inelastic events at small angles can be accounted for by the following way. First, the distribution measured by FD1-FD10 will be fit by a well-known function of θ, like an exponential, and will be extrapolated to $\theta = 0$. The magnitude of the correction is expected to be of order 1%. Second, more precise angular distributions can be drawn through the data from wire chambers. This procedure will yield more precise vertex recontsruction results and a good extrapolation to zero degree.

2. Each forward detector consists of 6 adjacent counters. The dead space between these counters may lead to loss of events. The correction in this case can be done by using wire chamber information. This correction has to be smaller than the ratio of dead space (= 0.2 mm) to active surface of the counter. Such a correction should be less than 0.1 %.

9 Conclusion

Apparatus is proposed which allows measurement of the total cross section in pp scattering at RHIC energies with a precision of order 1 % or better. It may be used in a whole region of RHIC energies ($50 \leq \sqrt{s}\ (GeV) \leq 500$). The ISD detector furnishes a veto trigger for ESD, measures and controls the beam luminosity, and reconstructs a vertex at IP with good resolution. ISD is based on robust and standard techniques of scintillating counters and strip chambers.

Future improvements

It is important to improve the beam parameters since they are very crucial for success of σ_T and ρ measurements. Let us enumerate some specific items:

1. Reduction of the longitudinal dimensions of the beam-overlap zone. The special attention should be taken on the z dimension of diamond region. We took above $\sigma_z = \pm 15\ cm$; while by using the Terwilliger scheme, the CERN people got $\pm 3\ cm$. We would like in future to reduce the longitudinal beam size to get closer to the latter number.

2. Reduction of the transverse beam size by stochastic cooling. In combination with the previous technique, this allows to suppress essentially all backgrounds.

3. Reduction of the transverse beam size or reducing off beam halo. This is the traditional technique of the beam scraper. Such a technique is beneficial in the case of high current, when the p beam develops a halo over a period of hours, resulting in increased background due to interactions with ambient material upstream of the Interaction Point.

References

[1] Experiment to Measure Total and Elastic pp Cross Sections at RHIC. Updated version, September 1995.

[2] S. van der Meer, CERN Internal Report ISR-PO/68-31 (1968), unpublished.

[3] C. Augier et al, CERN/PPE 94-160, Geneva, 6 October, 1994.

[4] J. Bosser et al., Nucl. Instr. Meth. A235 (1985) 475.

[5] K. M. Terwillinger, Proceedings of the International Conference on High-Energy Accelerators, CERN, 1958 (Geneva, 1959), p. 53.

[6] G. Carboni et al., Nucl. Phys. B254 (1985) 697.

[7] N. A. Amos et al., Phys. Rev. Lett. 63 (1989) 2784.

[8] S. White, Measurements of the pp Total Cross Sections at ($s = 1800$ GeV.) Preprint Fermilab-Conf-91/268-E, October 1991.

[9] G. Armson et al, CERN-EP/83-70, May 27th, 1983.

[10] C. Augier et al., Phys. Lett. B316 (1993) 448.

[11] N. A. Amos et al., Phys. Lett. B243 (1990) 158.

[12] G. Chiarelli, Fermilab-Conf-93/360-E, November 1993.

[13] U. Amaldi et al., Phys. Lett. B43 (1973) 231.

[14] N. A. Amos et al., Phys. Rev. Lett. 68 (1992) 2433.

[15] Particle Data, Phys. Rev. D. 54 (1996) 186.

[16] G. Bencze et al., Nucl. Instr. Meth. A357 (1995) 40 - 54.

[17] Collaboration TOTEM, Letter of Intent CERN/LHCC 97 - 49, LHCC/I11, 15 August, 1997.

[18] G. J. Alner et al., Z. Phys. C - Part. and Field. 33, (1986) 1.

[19] L. Baksay et al., Nucl. Phys. B141 (1978) 1.

Figure captions.

Fig 1. The $\mid t \mid$ dependence of the elastic pp differential cross section. Region I - a pure Coulomb scattering, II - Coulomb - Nuclear Interference region, III - diffraction scattering region, IV - hard scattering region.

Fig.2. The charged particle distribution versus rapidity in pp collision at $\sqrt{s} = 200\ GeV/c$ (open circles) and $\sqrt{s} = 546\ GeV/c$ (solid circles). The solid line is a fit to the experimental data in the range $1.8 \leq \eta \leq 4.6$. The dotted lines are gaussians, the dot-dashed lines show the linear extrapolation to η_{max}.

Fig.3. The angular distributions of elastic and inelastic events at $\sqrt{s} = 200\ GeV$.

Fig.4. Vacuum hardware parameters from DO magnet to experimental area and the layouts of Inelastic Scattering Detectors (FD1-10, CD1-2): top view (a) and side view (b).

Fig.5. The layout of FD (a) and CD (b) Inelastic Scattering Detectors.

Fig.6. The sketch of Cathode Strip Chambers (CSC).

Fig.7. The electronics scheme of ISD.

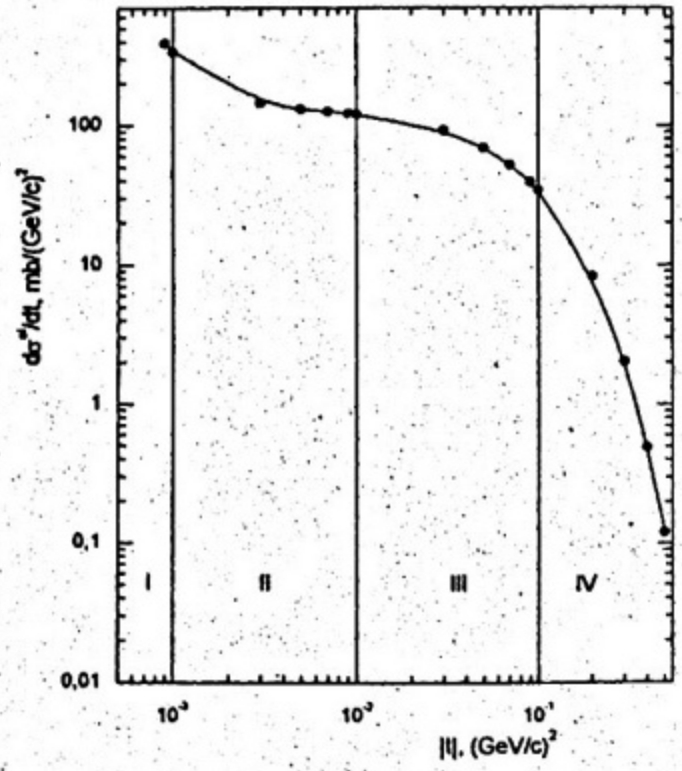
100
10
1
0,1
0,01
I
II
III
IV
10^{-3}
10^{-2}
10^{-1}
$|t|, (GeV/c)^2$
$d\sigma^{el}/dt, mb/(GeV/c)^2$

Fig. 1

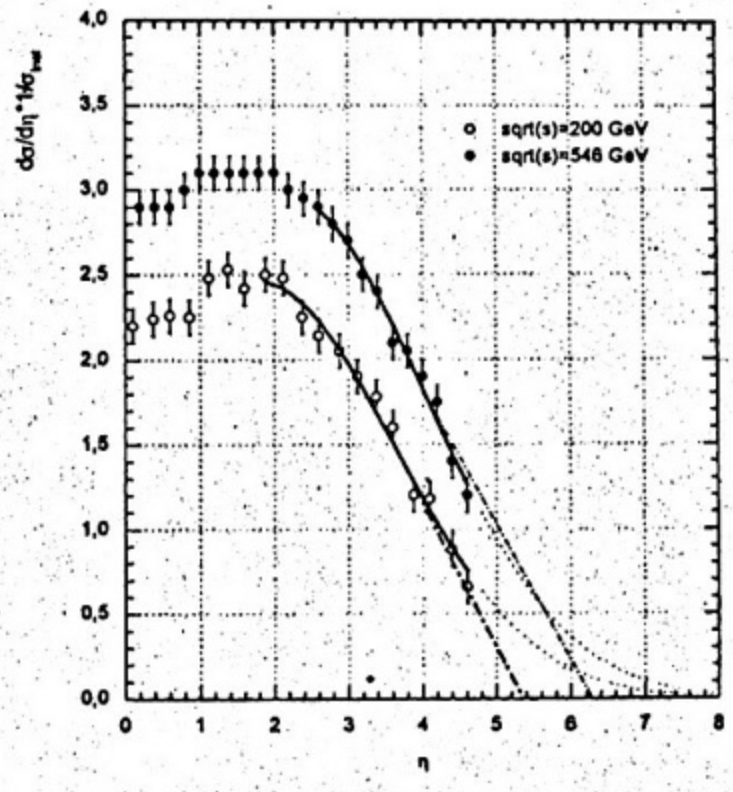
sqrt(s)=200 GeV
sqrt(s)=546 GeV
4,0
3,5
3,0
2,5
2,0
1,5
1,0
0,5
0,0
0
1
2
3
4
5
6
7
8
η
$d\sigma/d\eta * 1/\sigma_{inel}$

Fig. 2

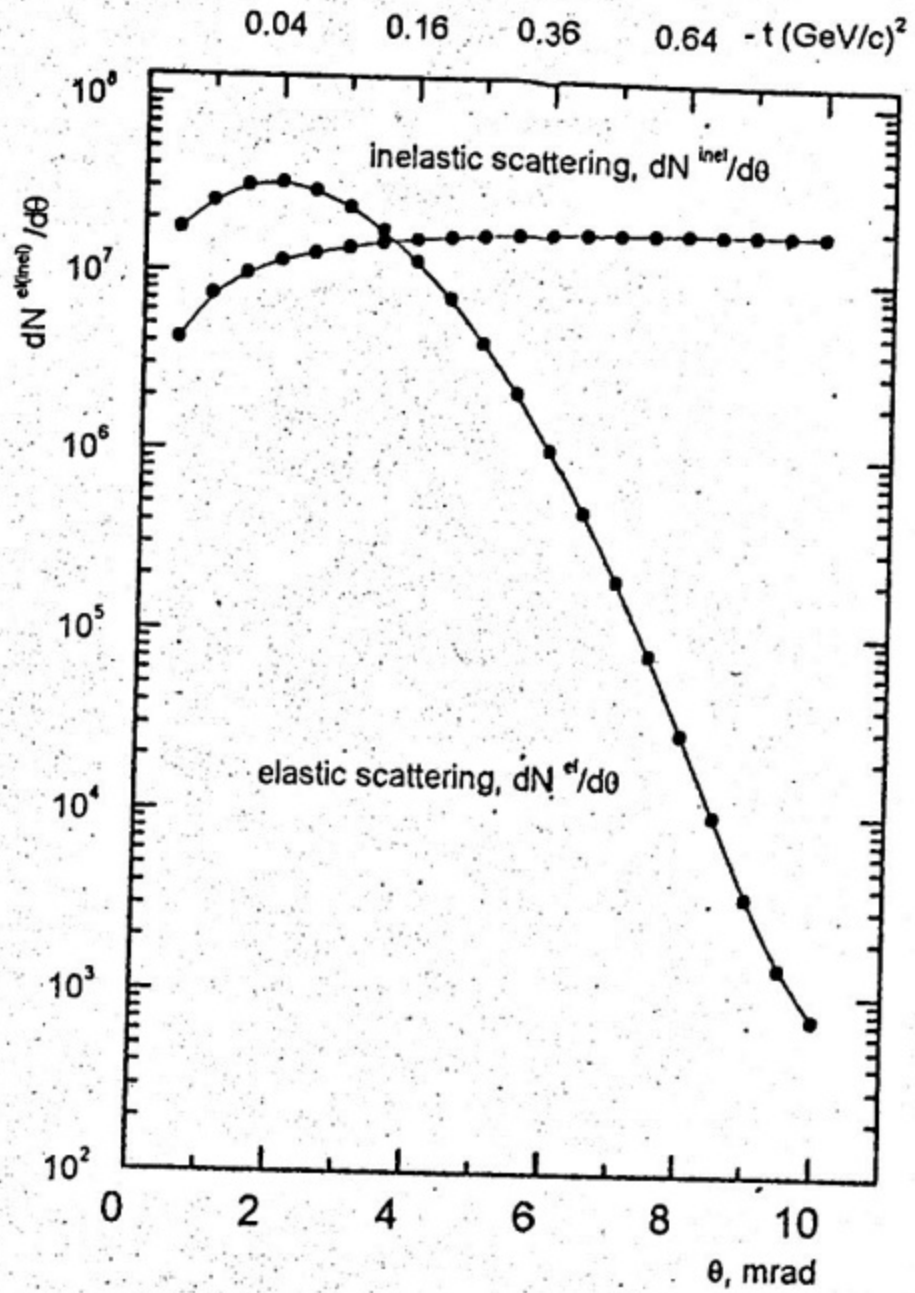
0.04
0.16
0.36
0.64
- t (GeV/c)²
10⁸
10⁷
10⁶
10⁵
10⁴
10³
10²
dN el(inel) /dθ
inelastic scattering, dN inel/dθ
elastic scattering, dN el/dθ
0
2
4
6
8
10
θ, mrad

Fig. 3

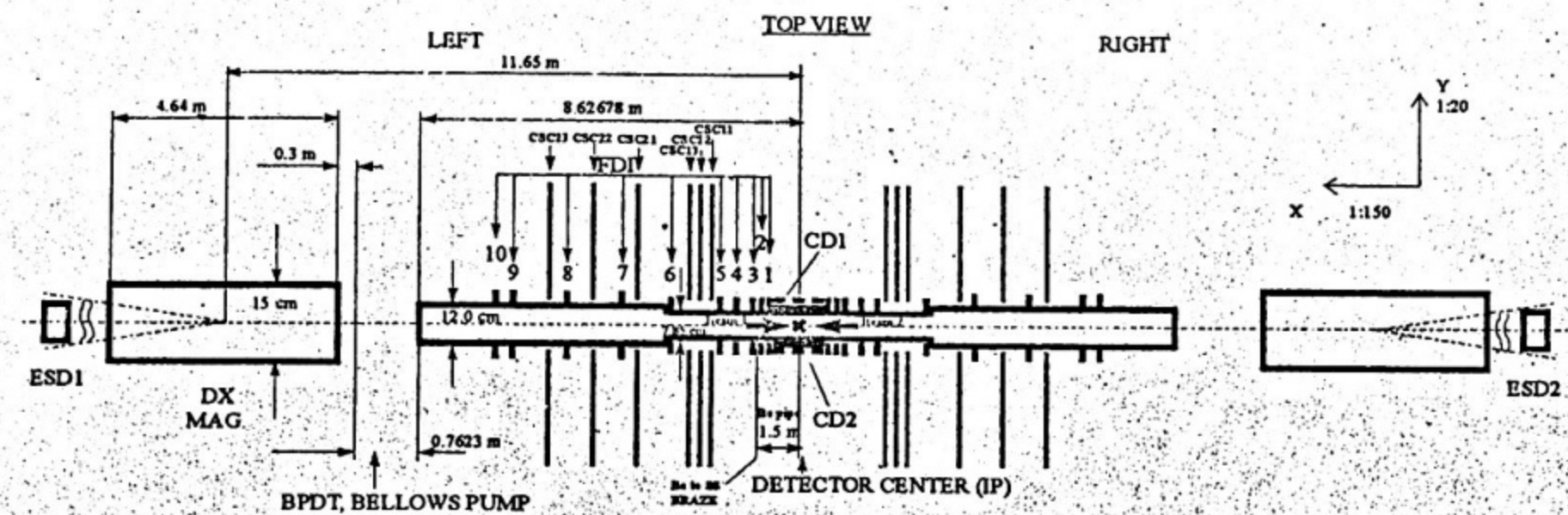
TOP VIEW
LEFT
RIGHT
11.65 m
4.64 m
8.62678 m
0.3 m
FDI
CD1
CD2
15 cm
120 cm
1.5 m
0.7623 m
ESD1
ESD2
DX
MAG
BPDT, BELLOWS PUMP
SYSTEM & VALVE
DETECTOR CENTER (IP)
Y
1:20
X
1:150

Fig. 4a.

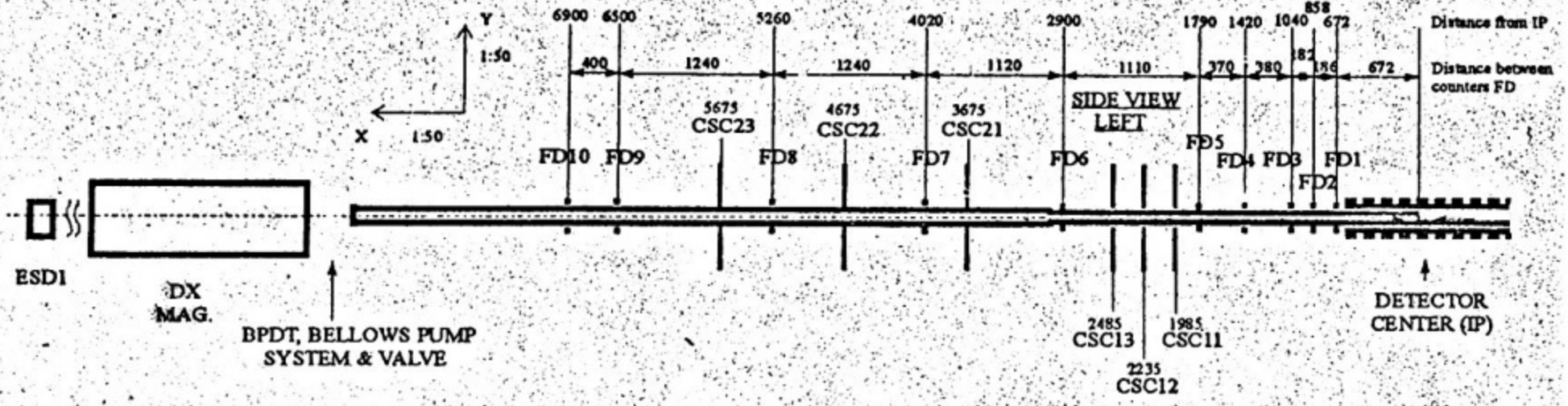
SIDE VIEW
LEFT
Distance from IP
Distance between
counters FD
6900
6500
5260
4020
2900
1790
1420
1040
858
672
400
1240
1240
1120
1110
370
380
182
156
672
5675
CSC23
4675
CSC22
3675
CSC21
FD10
FD9
FD8
FD7
FD6
FD5
FD4
FD3
FD2
FD1
2485
CSC13
1985
CSC11
2235
CSC12
ESD1
DX
MAG.
BPDT, BELLOWS PUMP
SYSTEM & VALVE
DETECTOR
CENTER (IP)
Y
1:50
X
1:50

Fig. 4b.

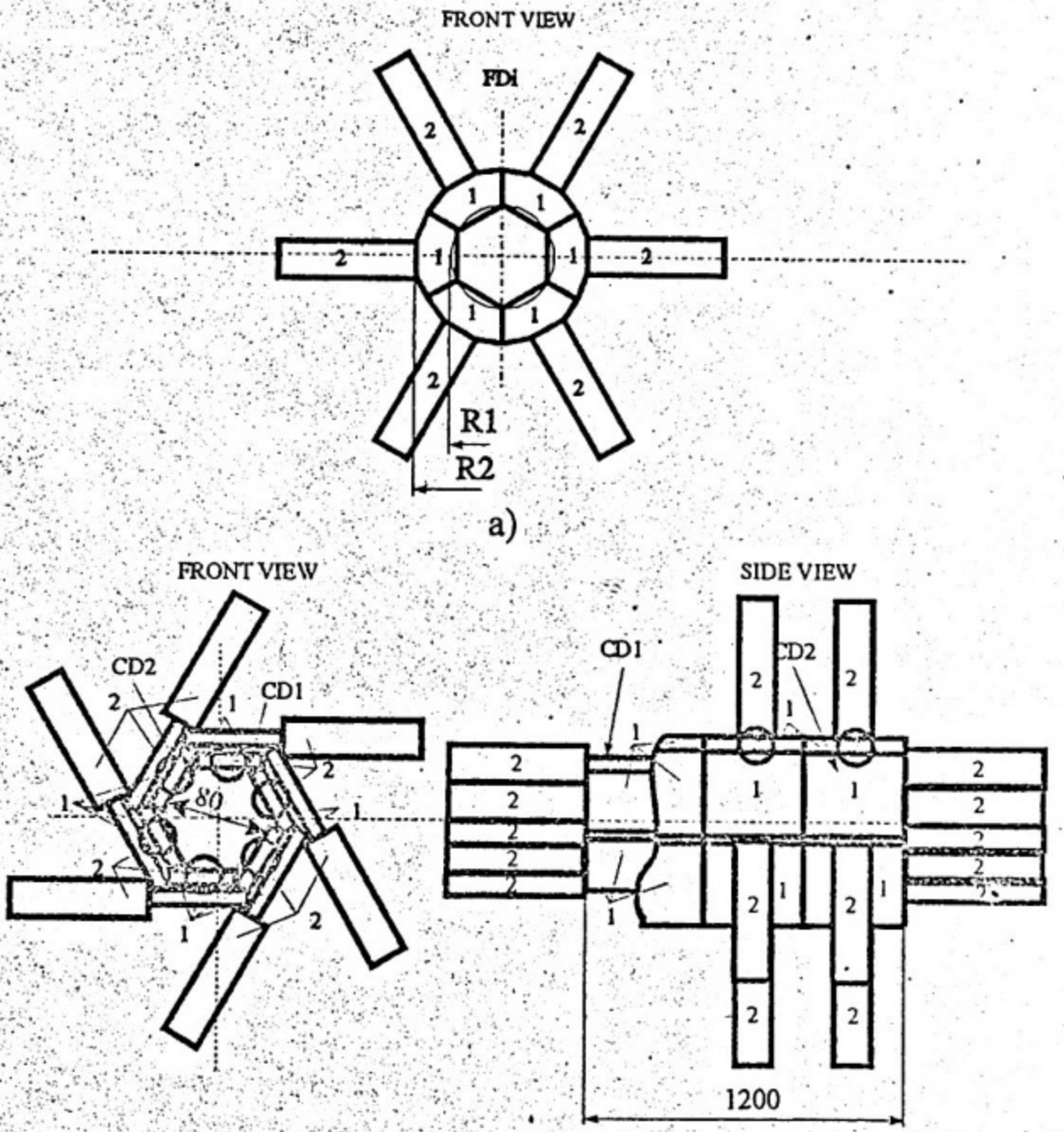

1 - scintillator, 2 - p.m. tube.

Fig. 5.

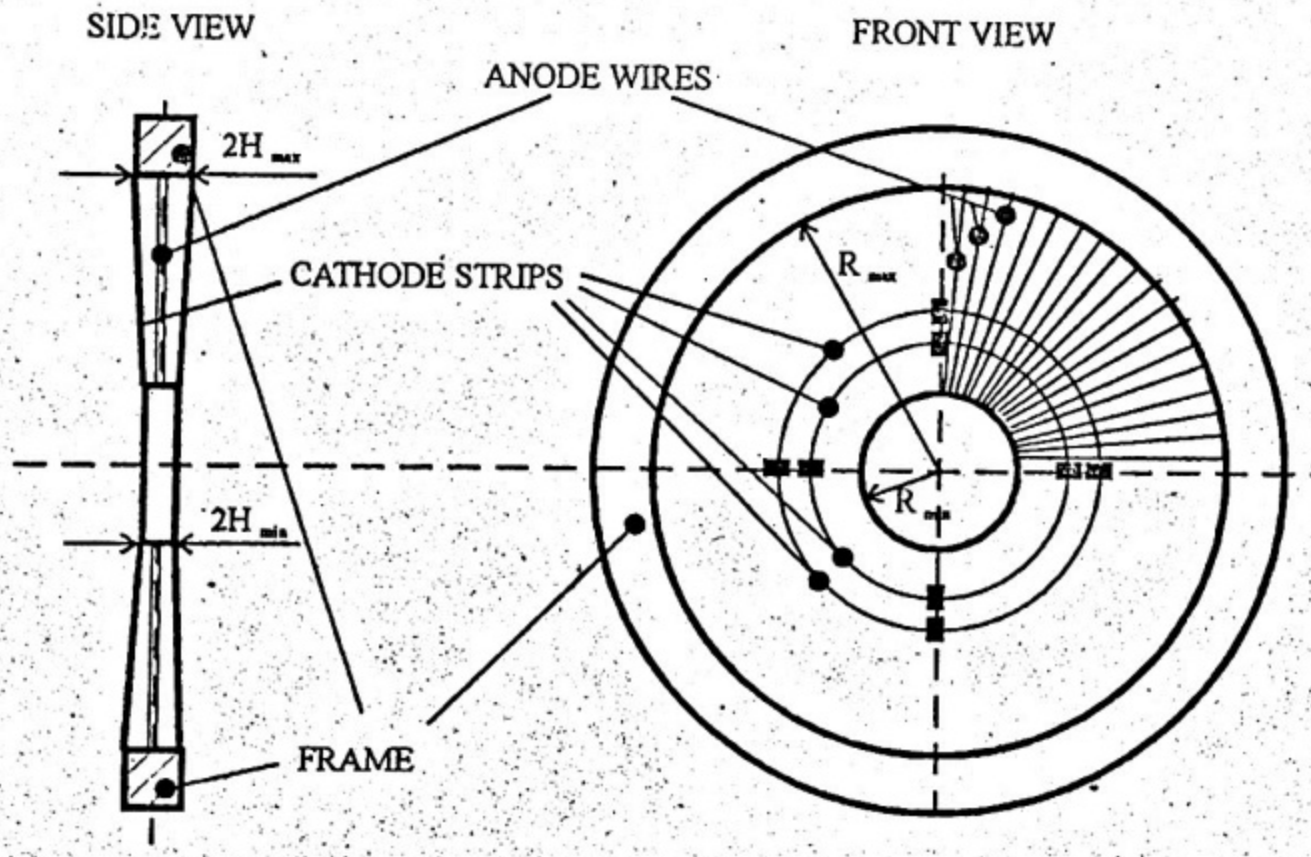
SIDE VIEW
FRONT VIEW
ANODE WIRES
2H max
CATHODE STRIPS
R max
2H min
FRAME

Fig. 6.

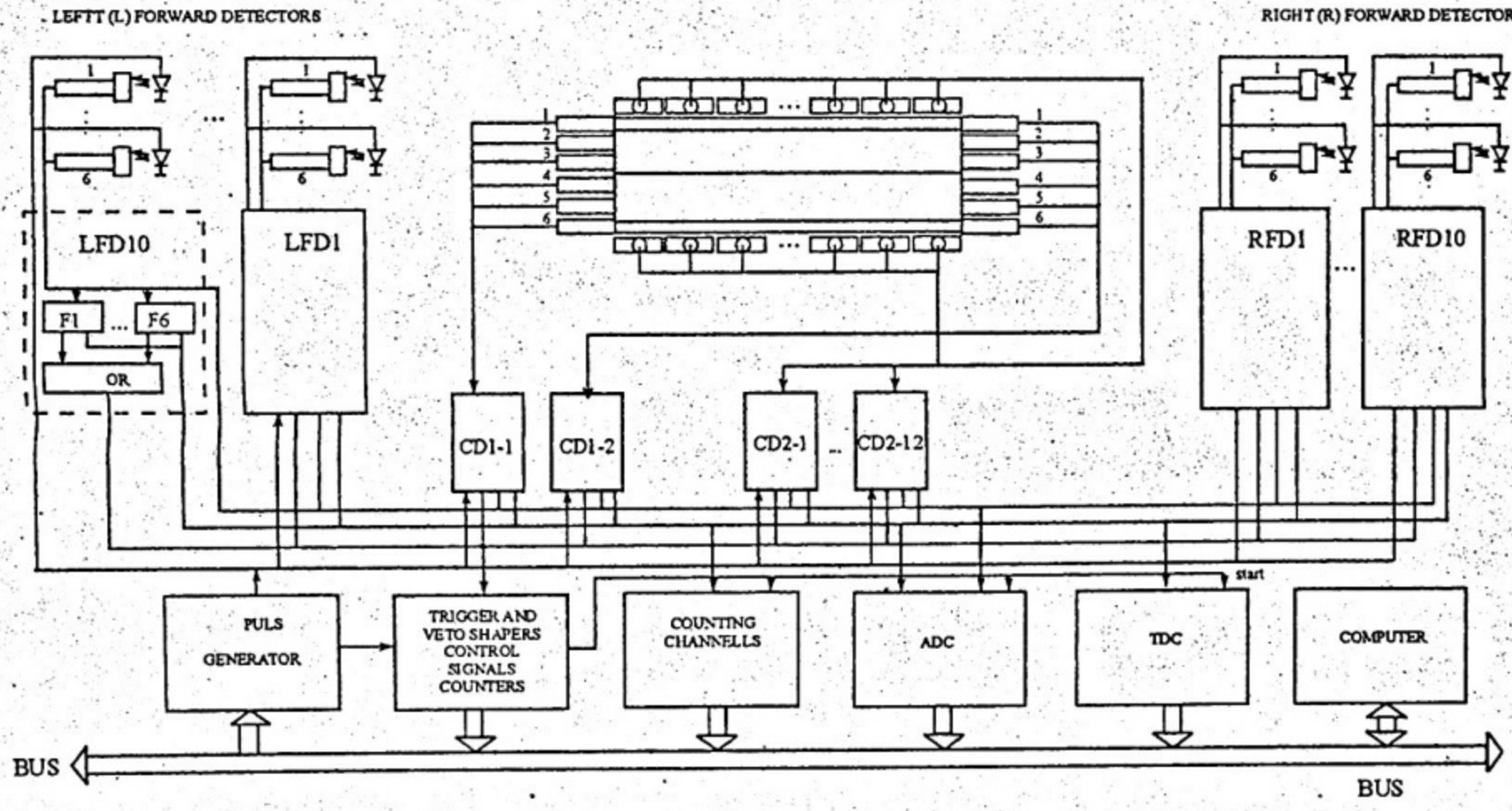

F - shaper, OR - logical "OR" scheme, ADC - amplitude - to - digit converter. ,TDC - time - to - digit converter.

Fig.7.

Алексей Александрович Богданов
Валерий Константинович Чернятин
Роберт Крин
Игорь Владимирович Главанаков
Владислав Анатольевич Григорьев
Влодек Гурин
Геннадий Николаевич Дудкин
Валерий Михайлович Емельянов
Владимир Александрович Каплин
Александр Иванович Каракаш
Юрий Федорович Кречетов
Геннадий Андреевич Науменко
Сандибек Байтемирович Нурушев
Александр Петрович Потылицын
Владимир Николаевич Падалко
Михаил Федорович Рунцо
Адам Руссек
Михаил Николаевич Стриханов

Детектор неупруго рассеянных частиц

для эксперимента pp2pp на ускорителе RHIC

Рукопись поступила в издательский отдел 14.09.2000
Ответственный за выпуск А.А. Богданов
Редактор Н.В. Шумакова
Лицензия ЛР №020676 от 09.12.92
Подписано в печать 29.09.2000 Формат 60x84 1/16
Объем 2,0 п.л. Уч-изд.л 2,0. Тираж 100 экз. Изд. № 008-2000
Заказ

Московский государственный инженерно-физический институт (технический университет). Типография МИФИ.
115409, Москва, Каширское шоссе., 31.